



Reductive Amination of Ketones with Benzylamine Over Gold Supported on Different Oxides

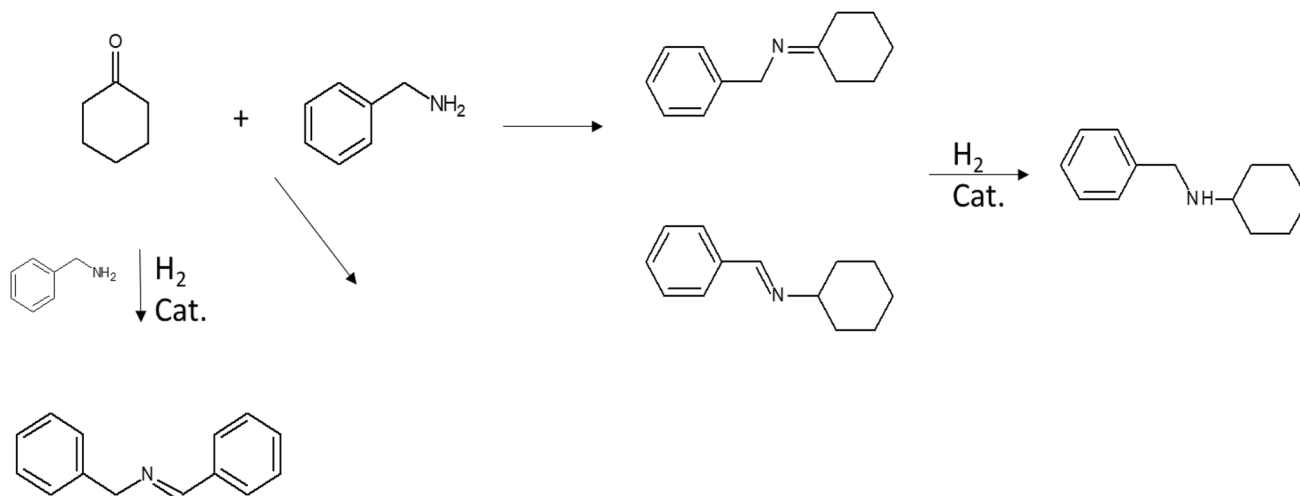
E. Kolobova¹ · P. Mäki-Arvela² · A. Pestryakov¹ · E. Pakrieva¹ · L. Pascual³ · A. Smeds² · J. Rahkila⁴ · T. Sandberg⁵ · J. Peltonen⁶ · D. Yu. Murzin²

Received: 5 June 2019 / Accepted: 15 July 2019
© The Author(s) 2019

Abstract

Reductive amination of cyclohexanone with benzylamine was investigated at 100 °C under 30 bar hydrogen in toluene with five different gold catalysts prepared by deposition–precipitation method and supported on TiO₂, La₂O₃/TiO₂, CeO₂/TiO₂, La₂O₃ and CeO₂. Size of metallic gold varied in the range of 2.6–3.6 nm. The best catalysts in reductive amination of cyclohexanone with benzylamine were 4 wt% Au/TiO₂ and 4 wt% Au/CeO₂/TiO₂ giving 72% and 79% yield of the desired amine. The most acidic and basic catalysts were also unselective and exhibited low activity towards imine hydrogenation. The best catalyst 4 wt% Au/CeO₂/TiO₂ gave in reductive amination of propiophenone 56% selectivity to the corresponding amine at 20% conversion in 5 h.

Graphical Abstract



Keywords Reductive amination · Gold catalysts · Cyclohexanone · Propiophenone

Electronic supplementary material The online version of this article (<https://doi.org/10.1007/s10562-019-02917-1>) contains supplementary material, which is available to authorized users.

✉ D. Yu. Murzin
dmurzin@abo.fi

Extended author information available on the last page of the article

1 Introduction

Secondary amines are important intermediates used for production of pharmaceuticals. Several methods can be used for their production, such as hydroamination of alkynes using homogeneous metal complexes [1], ethylmagnesiumation of imines with homogeneous metal complexes [2], reductive amination in ionic liquids [3], reductive allylation of amides

using homogeneous catalysts [4], as well as reductive amination using heterogeneous metal catalysts [5–7].

Hydroamination of alkynes has been conducted using titanium indenyl complexes. In the first step of the reaction 1-phenylpropyne reacted with benzylamine with $[\text{Ind}_2\text{TiMe}_2]$ complex as a catalyst at 105 °C in 2 h in toluene followed by hydrogenation of imine in methanol for 20 h using NaBH_3CN as a reducing agent in the presence of ZnCl_2 at 25 °C giving *N*-benzyl-1-phenylpropan-1-amine. As a result a mixture of regio-isomers was obtained [1]. In addition, α -ethyl-*N*-(phenylmethyl)benzenemethanamine was produced via ethylmagnesiumation (EtMgCl) of the corresponding imine in the presence of a homogeneous catalyst, zirconocene dichloride (di(cyclopentadienyl)zirconium(IV) dichloride, Cp_2ZrCl_2) in tetrahydrofuran under argon atmosphere giving 90% yield at 20 °C after 8 h [2].

N-benzyl-1-phenylpropan-1-amine with 86% yield after 3 h at room temperature has been synthesized via reductive allylation of *N*-benzylbenzamide using a homogeneous iridium complex as a catalyst in dichloromethane [4]. In addition, *N*-alkylation of aromatic alcohols over non-noble metal catalysts for production of amines such as via hydrogen borrowing mechanism [8], was done with benzyl alcohol and cyclohexylamine as reactants over NiCuFeO in xylene under reflux giving 89% yield of cyclohexylbenzenemethanamine in 24 h.

Heterogeneous catalysts, such as Pd/C , Pt/C and Rh/C [5] and Au/TiO_2 [6] have been used in reductive amination of ketones. In particular Pd/C , Pt/C and Rh/C [5] were active in amination of aldehydes and ketones in the absence of hydrogen, requiring, however, high pressure of CO . Reductive amination of benzaldehyde with *p*-anisidine was performed in the presence of 95 bar CO at 140 °C in tetrahydrofuran over Rh/C catalyst giving 50% of the corresponding amine after 42 h [5]. A carbon based solid acid catalyst of the overall composition $\text{CH}_{0.6}\text{O}_{0.35}\text{S}_{0.14}$ prepared by sulfonation of naphthalene with sulfuric acid at 200–300 °C [9] was used in reductive amination of cyclohexanone with benzylamine allowing 90% yield of *N*-benzylcyclohexylamine in 10 min at room temperature with NaBH_4 as a reducing agent [10]. Au/TiO_2 was reported as an efficient catalyst for reductive amination of cyclohexanone with benzylamine at 60 °C in *tert*-butanol using formic acid as a hydrogen source [6]. Unsupported ionic liquid (carboxymethyl)-1-methyl-1*H*-imidazol-3-ium-bis(trifluoromethyl)sulfonylamine has also been applied as a catalyst in the same reaction using formic acid and triethylamine as hydrogen sources at 40 °C in acetonitrile as a solvent [3]. The authors [3] achieved the yield of amine of 30% after 5 h.

Imines have been hydrogenated using isopropanol as a hydrogen source in transfer hydrogenation and Funk's iron complex together with $\text{Fe}(\text{acac})_3$ as a catalyst under nitrogen atmosphere at 110 °C under 48 h facilitating formation of

N(*E*)-*N*-(1-phenylpropylidene)-benzenemethanamine with 98% yield [11].

Based on a recent study [6], describing Au/TiO_2 and formic acid as a catalyst and a hydrogen source in reductive amination of cyclohexanone with benzylamine, it was decided to explore catalytic behavior of different Au supported catalysts in reductive amination of cyclohexanone and propiophenone with benzylamine using instead of formic acid as a hydrogen source molecular hydrogen, which has clear advantages in the case of industrial implementation compared to formic acid, namely lower costs and no CO_2 release.

2 Experimental

2.1 Catalyst Preparation and Characterization

Aeroxide[®] Titania P25 (Evonik Degussa GmbH), lanthanum(III) oxide (Merck), cerium(IV) oxide (Merck) were used as supports. For comparative studies, titania was modified with ceria and lanthana by impregnating with aqueous solutions of the corresponding nitrates (molar ratio $\text{Ti/M} = 40$, $\text{M} = \text{Ce}$ or La). The catalysts (4wt% Au/TiO_2 , 4wt% $\text{Au/M}_x\text{O}_y/\text{TiO}_2$ (where $\text{M}_x\text{O}_y = \text{CeO}_2$ or La_2O_3), 4wt% Au/CeO_2 and 4wt% $\text{Au/La}_2\text{O}_3$) were prepared by the deposition–precipitation method with urea, previously described in ref. [12]. Gold(III) chloride trihydrate (Merck) was used as a gold precursor. The nominal gold content in all catalysts was 4 wt%. After the gold deposition and drying procedure, the materials were treated in a reducing atmosphere (H_2) at 300 °C for 1 h.

The specific surface area (S_{BET}) of the supports and catalysts was measured by nitrogen adsorption method (“TriStar 3000” analyzer, Micromeritics, USA). The phase composition of the materials was studied by XRD (Philips XPERT PRO diffractometer). The measured diffractograms were analyzed with the ICDD-2013 powder diffraction database and Inorganic Crystal Structure Database (ICSD) [13]. Catalysts morphology and the gold cluster size were investigated by transmission electron microscopy and scanning transmission electron microscopy-High Angle Annular Dark Field (JEOL JEM-2100F). The gold content was measured by energy dispersive spectroscopy (JEOL JEM-2100F with an Oxford INCA X-sight system detector) and inductively coupled plasma optical emission spectrometry (Perkin Elmer ICP-OES Optima 3300 DV spectrometer). The electronic state of gold on the support surface was determined by XPS (SPECS Surface Nano Analysis GmbH, Berlin, Germany). The concentration of basic and acid sites, and their distribution in supports and catalysts were investigated by temperature programmed desorption (TPD) of CO_2 (Autochem 2900

apparatus) and NH₃ (Chemosorb–chemisorption analyzer), respectively.

Details on the catalysts preparation and characterization are reported in the Electronic supplementary material.

2.2 Catalyst Testing

Reductive amination of cyclohexanone (Sigma Aldrich $\geq 99.5\%$) and propiophenone (Kebo Lab $> 99\%$) with benzylamine (Fluka $\geq 99\%$), was performed in an autoclave using toluene as a solvent. In a typical experiment 6.6 mmol of ketone and 6.6 mmol of benzylamine in 50 ml solvent were mixed with 100 mg of catalyst. Thereafter, the reactor was flushed with hydrogen and after reaching the desired temperature and pressure, the reaction was started. The stirring rate was 900 rpm and small catalyst particles, below 63 μm were used to suppress the external and internal mass transfer limitations. The samples were taken from the reactor and analyzed by GC equipped with a FID detector and a capillary column, HP-5 (length 30 m, internal diameter 320 μm , film thickness 0.50 μm) with the following temperature programme: 100 °C (5 min)–5 °C/min–320 °C (5 min). The products were confirmed by GC–MS.

NMR spectra were recorded on a Bruker AVANCE III spectrometer equipped with a BB/1H SmartProbe operating at 500.10 MHz (¹H) and 125.8 MHz (¹³C). 15N-1H HMBG were recorded on a Bruker AVANCE III spectrometer equipped with a Prodigy BBO CryoProbe operating at 500.20 MHz (¹H) and 50.59 MHz (¹⁵N). The spectra were calibrated against an internal standard TMS (tetramethylsilane, $\delta_{1\text{H}} = 0.0$ ppm, $\delta_{13\text{C}} = 0.0$ ppm) or residual solvent signals (DMSO-*d*₆: $\delta_{1\text{H}} = 2.50$ ppm, $\delta_{13\text{C}} = 39.5$ ppm). All spectra were recorded at 25 °C and a standard set of ¹H, ¹³C, DQF-COSY, HSQC (multiplicity edited, CH/CH₃ signals positive, CH₂ signals negative) and HMBG (with a threefold low-pass J-filter to suppress one-bond correlations) experiments was acquired.

2.3 Quantum Mechanical Calculations

The stability of imine structures (1D) (*E*)-*N*-(cyclohexylmethyl)-1-phenylpropan-1-imine and (1C) *N*-(cyclohexylmethyl)-1-phenylpropan-1-imine was studied by a multi-level deterministic structural optimization using the Forcite, *Conformers* and *DMol3* modules in the software *Materials studio version 7.0* [14, 15]. At molecular mechanics (MM) level, the Universal Force Field was applied as implemented in the *Conformers module*. The most stable conformers were optimized with density functional theory applying the B3LYP hybrid functional [16–19] the DNP basis set and Grimme's method for DFT-D (dispersion) correction [20] as implemented in the *DMol3 module*.

Vibrational frequencies were also calculated in order to obtain thermodynamic data of the stabilities.

3 Results and Discussion

3.1 Catalyst Characterization Results

The phase composition of the studied catalysts was investigated by XRD (Fig. 1). Analysis of diffractograms of 4wt% Au/TiO₂, 4wt% Au/La₂O₃/TiO₂, 4wt% Au/CeO₂/TiO₂ and their corresponding supports (Fig. 1a, b, c) showed absence of any diffraction peaks characteristic for gold, ceria or lanthana, implying that their size is lower than 3–4 nm (i.e. sensitivity of XRD) or that they are X-ray amorphous. For these samples, only reflections characteristic of titania (P25) were observed [21]. Previously, this was also reaffirmed by XRD-SR [22], where the reflections related to additives (CeO₂) were only detected for 4wt% Au/CeO₂/TiO₂.

The XRD pattern of CeO₂ (Fig. 1d) revealed all of the major characteristic peaks of CeO₂ corresponding to the (111), (200), (220), (400), (311), (222) and (420) planes, which are very close to the face centered cubic CeO₂ crystal [23] indicating the cubic fluorite structure (JCPDS file No: 81-0792). No changes in the phase composition or the support structure were detected after gold deposition. Moreover, no reflections related to the Au NPs were observed as mentioned above.

The diffractogram of La₂O₃ (Fig. 1e) consisted of peaks related to hexagonal [24] and monoclinic [25] polymorphs of La₂O₂(CO₃). Deposition of gold on La₂O₃ surface leads to a change in its structure and composition. The diffractogram of 4 wt% Au/La₂O₃ consisted of peaks related to La(OH)₃ (hexagonal) [26] and La₂(CO₃)₂(OH)₂ (orthorhombic) [27], while no peaks related to Au were seen.

The highest specific surface area (S_{BET}) was measured for 4 wt% Au/TiO₂ being 50 m²/g_{cat} (Table 1). Loading of 4 wt% Au on TiO₂ decreased its surface area by 15%. Both addition of CeO₂ and La₂O₃ decreased the specific surface area of 4wt% Au/La₂O₃/TiO₂ and 4wt% Au/CeO₂/TiO₂ in comparison with 4wt% Au/TiO₂. The lowest specific surface area was determined for 4wt% Au/La₂O₃ and 4wt% Au/CeO₂. In comparison with data reported by Demidova et al. [28] the S_{BET} of La₂O₃ and CeO₂ are much lower than in the current work, however, following the same trends.

The mean size of gold particle was determined by TEM (Table 1, Electronic supplementary material, Figure S1). The largest value was measured for 4wt% Au/La₂O₃, which also exhibited the lowest specific surface area. On the other hand, the average gold particle sizes for other studied catalysts were in the narrow range of 2.6–2.9 nm. Morphology of different catalysts was also investigated

Fig. 1 XRD patterns for 4wt% Au/TiO₂ (a), 4wt% Au/CeO₂/TiO₂ (b), 4wt% Au/La₂O₃/TiO₂ (c), 4 wt% Au/CeO₂ (d) and 4wt% Au/La₂O₃ (e) versus corresponding supports

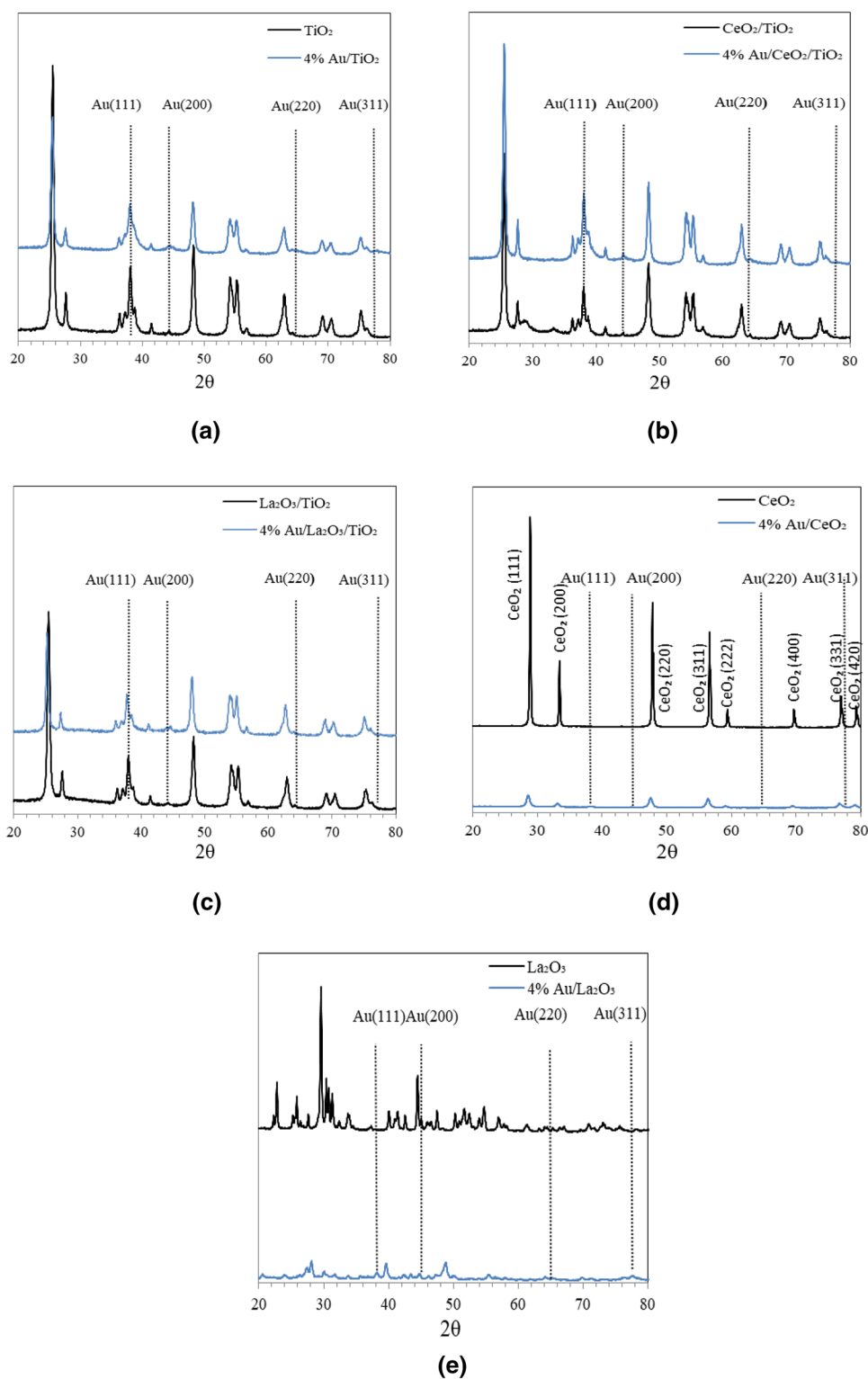


(Fig. S1). In particular, 4 wt% Au/TiO₂ exhibited irregular shape particles in the range of 10–35 nm (Fig. S1a). Morphology of 4 wt% Au/CeO₂/TiO₂ and 4 wt% Au/La₂O₃/TiO₂ did not change remarkably after ceria and lanthana modification because to their small amounts (Fig. S1 b, c).

Irregular shaped particles in 4 wt% Au/CeO₂ exhibited the size of 8–25 nm (Fig. S1d). Particles in 4 wt% Au/La₂O₃ were not clearly separated in the TEM image most probable due to changes in La₂O₃ after gold modification (Fig. S1 e) identified by XRD (see above).

Table 1 Specific surface area of the supports and catalysts, average Au particles size

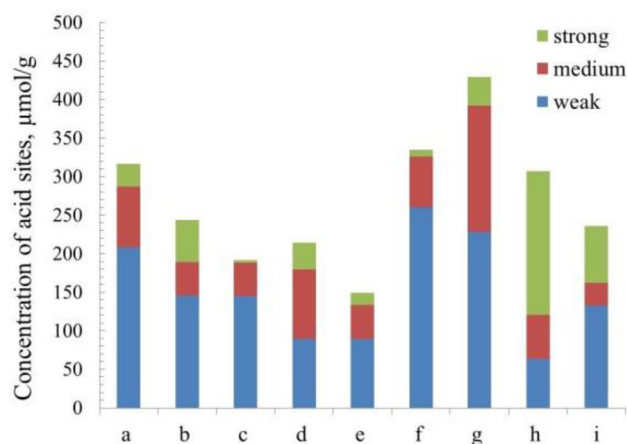
Catalyst	S_{BET} , m^2/g	Au average particle size, nm
TiO ₂	54	—
La ₂ O ₃	9	—
CeO ₂	37	—
La ₂ O ₃ /TiO ₂	48	—
CeO ₂ /TiO ₂	48	—
4wt% Au/La ₂ O ₃ /TiO ₂	43	2.6
4wt% Au/CeO ₂ /TiO ₂	46	2.8
4wt% Au/TiO ₂	50	2.9
4wt% Au/La ₂ O ₃	10	3.6
4wt% Au/CeO ₂	38	2.6

Table 2 Concentration of acidic sites of the catalysts determined by TPD of ammonia

Sample	Concentration of acid sites, $\mu\text{mol}/\text{g}$			
	Weak	Medium	Strong	Total
TiO ₂	208	79	30	317
La ₂ O ₃	89	91	34	214
CeO ₂	89	45	15	149
La ₂ O ₃ /TiO ₂	145	43	4	192
CeO ₂ /TiO ₂	146	43	55	244
4wt. %Au/La ₂ O ₃ /TiO ₂	63	58	103	307
4wt. %Au/CeO ₂ /TiO ₂	228	164	37	429
4wt. %Au/TiO ₂	260	66	9	335
4wt. %Au/La ₂ O ₃	—	852	2548	3400
4wt. %Au/CeO ₂	133	29	74	236

It is noted in the literature [28–30] that the acid–base properties of the support play a very important role in the amination of oxygen-containing compounds. The acidic and basic properties of supports and respective gold catalysts were investigated by NH₃-TPD (Table 2, Fig. 2) and CO₂-TPD (Table 3, Fig. 3).

Three types of acid sites with different strength and concentrations were observed for the initial supports (Table 2, Fig. 2). Among the used supports, unmodified titania has the highest acidity, characterized by the presence of both weak and medium strong Brønsted acid sites (acidic OH groups), according to [31–33]. The presence of strong acid sites may be due to the existence of Lewis (aprotic sites—tetrahedral coordinated Ti⁴⁺) and/or Brønsted sites. The total acidity of ceria and lanthana was 1.5 and 2.1 fold lower than the acidity of titania. The main difference is in the concentration of weak acid sites the amount of which for TiO₂ is 2.3 fold higher than for CeO₂ and La₂O₃, both latter ones exhibiting the same amounts. In contrast to ceria, the concentration

**Fig. 2** The distribution of the acid sites in strength and concentration for: a—TiO₂; b—CeO₂/TiO₂; c—La₂O₃/TiO₂; d—La₂O₃; e—CeO₂; f—4wt% Au/TiO₂; g—4wt% Au/CeO₂/TiO₂; h—4 wt% Au/La₂O₃/TiO₂; i—4wt% Au/CeO₂.**Table 3** Concentration of basic sites of the catalysts determined by TPD of CO₂

Catalyst	Concentration of basic sites, $\mu\text{mol}/\text{g}$			
	Weak	Medium	Strong	Total
TiO ₂	29	51	5	88
La ₂ O ₃	34	29	21	84
CeO ₂	45	54	23	122
La ₂ O ₃ /TiO ₂	56	46	17	119
CeO ₂ /TiO ₂	27	40	3	70
4wt% Au/La ₂ O ₃ /TiO ₂	38	46	76	161
4wt% Au/CeO ₂ /TiO ₂	60	63	31	153
4wt% Au/TiO ₂	15	41	17	73
4wt% Au/La ₂ O ₃	7	1488	28	1523
4wt% Au/CeO ₂	92	92	46	230

of medium and strong acid sites for lanthana was slightly higher than for titania.

After modification of the pristine titania surface with ceria and lanthana, a decrease in the concentration of both weak and medium acidic centers was observed, which is caused by dehydration of the surface under high temperature (550 °C) during preparation. In the case of the Ce-modified material, the concentration of strong acid centers increases almost two fold, compared to modification with lanthana, for which a sevenfold decrease in the concentration of strong acid sites was observed. It should be noticed that on the contrary to lanthana ceria is a reducible oxide with variable valence states. It can be suggested that after modification of titania with ceria, new Lewis acid sites Ce⁴⁺/Ce³⁺ can be formed, which presence being indirectly confirmed by TPR [34]. Deposition of gold on the supports

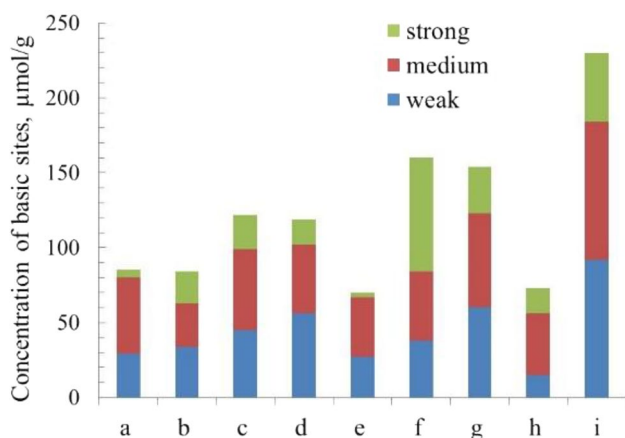


Fig. 3 The distribution of the basic sites in strength and concentration for: a—TiO₂; b—La₂O₃; c—CeO₂; d—La₂O₃/TiO₂; e—CeO₂/TiO₂; f—4wt% Au/La₂O₃/TiO₂; g—4wt% Au/CeO₂/TiO₂; h—4wt% Au/TiO₂; i—4wt% Au/CeO₂

results in redistribution of acid sites strength. This was most pronounced for 4wt% Au/La₂O₃, which acidity increased 16 fold compared with the corresponding support. Such significant changes are most likely associated with changes in the phase composition of lanthana after gold deposition (formation of lanthanum hydroxide and hydroxycarbonate observed by XRD, Fig. 1e). For all other studied catalysts, acidity alteration was much less noticeable and was not associated with changes in the phase composition according to XRD (Fig. 1). For 4wt% Au/TiO₂ the amount of weak sites moderately increased, while the concentration of medium sites slightly decreased, at the same time strong acid sites almost vanished. Similar trends in the change of support acidity after the introduction of the metal were previously discussed [35–37]. The origin of such changes was related to the mutual influence of the support and the metal crystallites on each other through their interactions at the catalyst preparation step. Furthermore, it was found [38–41] that during the gold deposition, the support surface is protonated, which leads to formation of additional OH groups, which can remain on the surface even after drying and redox pretreatments. Moreover, a part of the acid sites previously present on the surface can be blocked by formed gold nanoparticles. The amount of blocked sites depends on the nanoparticles size. Moreover, acidity can also affect the particle size, as previously found [42]. For Ce-modified titania catalysts, a decrease in the amount of strong acid sites after deposition of gold was also observed. In this case, however, the concentration of weak and medium acid sites increases. For 4wt% Au/La₂O₃/TiO₂ and 4wt% Au/CeO₂ the concentration of strong acid sites significant increased. When comparing XPS (Table 4) and NH₃-TPD (Table 2) data, it can be assumed that a part of these sites (39 μmol/g) is due to the presence of Au⁺, which are Lewis acid sites, while another

Table 4 Contribution of electronic states of gold calculated in accordance with XPS for studied catalysts

Sample	Au ^(0, +1, +3 or d-) content in the samples, %			
	Au ⁰ (84.1– 84.3 eV) ^b	Au ⁺ (85.0– 85.3 eV) ^b	Au ³⁺ (86.0– 86.3 eV) ^b	Au _n ^{d-} (83.3– 83.5 eV) ^b
4wt% Au/TiO ₂ ^a	74	15	11	0
4wt% Au/CeO ₂ /TiO ₂	68	20	12	0
4wt% Au/La ₂ O ₃ /TiO ₂ ^a	81	19	0	0
4wt% Au/La ₂ O ₃	50	12	0	38
4wt% Au/CeO ₂	57	21	0	22

^aFrom [34]

^bRefer to BE data from literature [34–61]

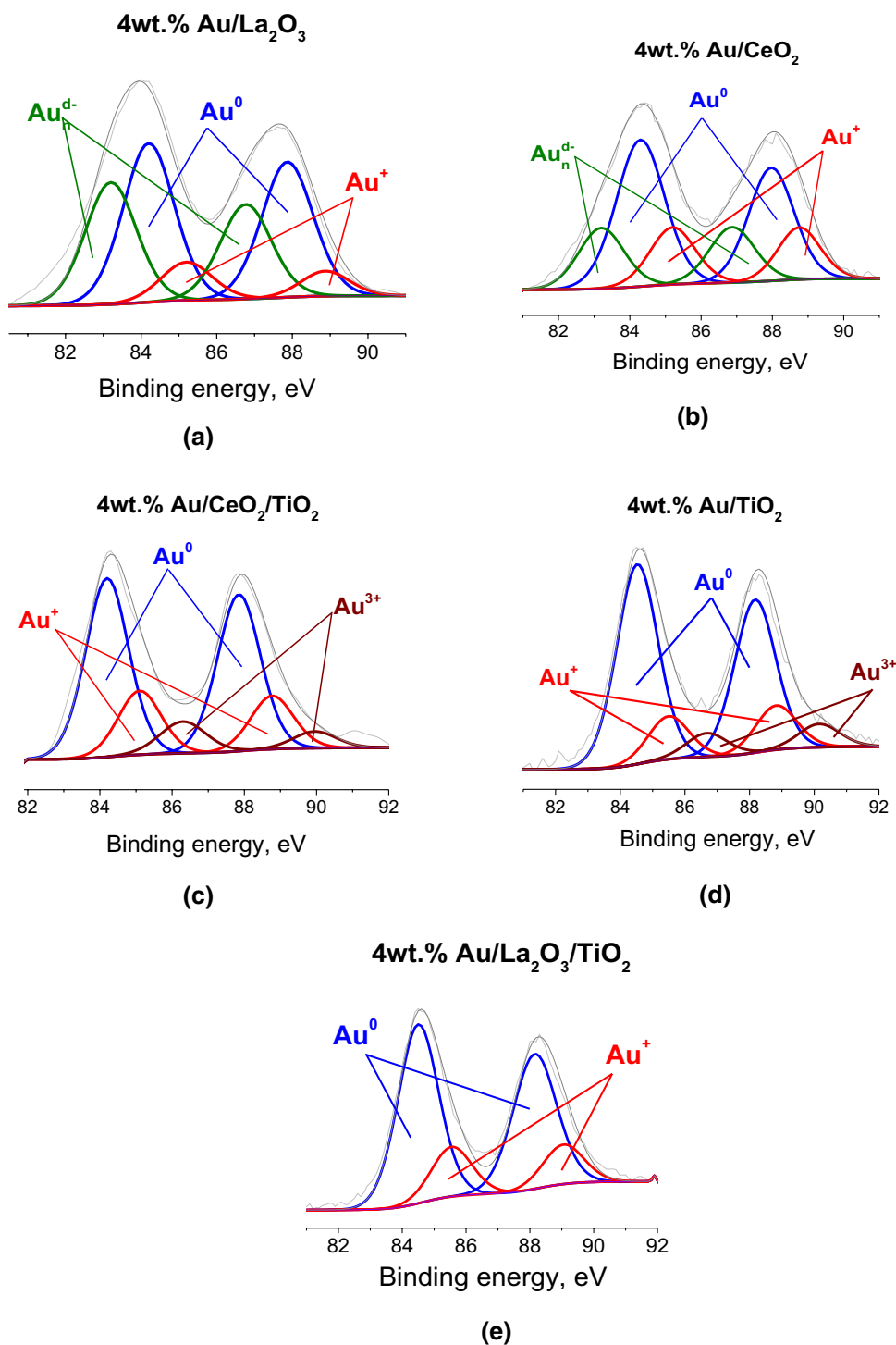
part is associated with Brønsted acidity and belongs to the support or the modifier. As for the acid sites of weak and medium strength, the amount of weak ones decreased for 4wt% Au/La₂O₃/TiO₂ and increased for 4wt% Au/CeO₂, while that of medium strong sites varied opposite to the weak ones.

According to the literature [43–46] CO₂ adsorption on metal-oxide materials results in formation of various carbonate species (bicarbonate, bidentate and monodentate carbonates), which are desorbed at different temperatures giving information about the strength and nature of the basic sites. CO₂ desorption in the low-temperature range (25–200 °C) is usually associated with the interactions of CO₂ with surface hydroxyl groups, which are basic sites of weak strengths. Medium strong basicity is related to the presence of metal-oxide pairs, in this case CO₂ desorption is observed in the range of 200–400 °C. Desorption peaks appearing in the range of 400–600 °C are caused by monodentate carbonate species formed on low-coordination oxygen anions which correspond to strong basic sites.

Three types of basic sites of different strength and concentrations were observed on the surface of studied supports in similar temperature ranges mentioned above (Table 3, Fig. 3). Among the used supports, CeO₂ and La-modified titania possess the highest and approximately the same basicity, with a small difference in the distribution of the basic sites in strength. For ceria weak/medium/strong site ratio is 2:2:1, while for La₂O₃/TiO₂, the ratio is 3:3:1. Titania and lanthana have intermediate basicity, for them the W/M/S ratio is 6:10:1 and 2:1:1, respectively. The lowest basicity was determined for Ce-modified titania, with the predominant contribution of the basic sites of medium strength (W/M/S ratio is 9:13:1).

Similar to acidic properties, after gold deposition a redistribution of basic sites was observed. For almost all studied catalysts, except 4wt% Au/TiO₂, a significant increase in the concentration of the basic sites was

Fig. 4 XPS results from different catalysts (a–e). **d** and **e** from [34]



observed compared to the corresponding supports, while the number of strong basic sites increased for all materials without any exception. Since the acid–base properties of materials are interrelated, such changes could occur for the reasons described above for acidity. The 18-fold increase in the basicity of 4wt% Au/La₂O₃ after gold deposition should be noted separately, associated with changes in the phase composition as described above for acidity.

Moreover, CO₂ desorption can be originated from carbonates, which are incorporated in the structure of lanthanum hydroxycarbonate. Thus, evaluation of basic sites is not straightforward, as these residual carbonates contribute to the overall released CO₂ in addition to carbon dioxide desorbed from basic sites. Furthermore, these data explain the formation of Au_n^{d-} sites (38%, Table 4, Fig. 4a) due to increased interactions between gold and the support

accompanied by changes in the structure and phase composition of the support.

XPS was used to determine the electronic state of gold. XPS spectra of Au_{4f} are shown in Fig. 4. A relative atomic concentration of various electronic states of gold, as well as the corresponding binding energies (BE), identified according to the literature [25–33, 47–61] are given in Table 4. Relative values of the various gold states depend strongly on the support nature. On the surfaces of all studied materials, most of gold (50–81%) is in a metallic state with BE (Au_{4f_{7/2}}) in the range of 84.1–84.3 eV, part of gold (12–21%) is present as Au⁺ with BE (Au_{4f_{7/2}}) in the range of 85.0–85.3 eV. In the case of unmodified and Ce-modified samples, another state related to Au³⁺ with BE of Au_{4f_{7/2}} = 86.1 and 86.2 eV appears in XPS spectra (11 and 12%, respectively). It is notable that for 4wt% Au/La₂O₃ and 4wt% Au/CeO₂ within BE range 83.3–83.5 eV, related to Au_n^{d-} states (38 and 22%, respectively), was observed. Such a shift towards lower BE as compared with the metallic state can be explained by several reasons. A negative particle charge may occur due to an electron transfer from the support to gold [54, 55, 60]. Another possible explanation is stronger interactions between gold and the support accompanied by local changes in the structure and phase composition of the support [43, 44, 48]. Finally, the particle shape determined by the size of gold nanoparticles may also be a reason of a lower BE shift [57].

3.2 Catalytic Results

3.2.1 Reductive Amination of Cyclohexanone

The results revealed that imines 1C/1D were instantaneously formed already after mixing of cyclohexanone with benzylamine at room temperature. According to GC analysis high conversion of cyclohexanone was obtained already after few minutes when a mixture of reactants and a solvent was prepared. Since the imine formation kinetics was very rapid, it was not quantified. Two different imines were formed, 1C and 1D (Table 5, Fig. 5) with D being the main product in line with quantum mechanical calculations for the Gibbs free energy also showing that this product is more stable than 1C by 19.5 kJ/mol at DFT/B3LYP/DNP level (Fig. 6). Standard thermodynamic quantities in the range 275–475 are shown in Table 6. At 298.15 K, the Gibb's free energy was 620.3 and 614.4 kJ/mol for the two conformers of the 1D structure and 613.8 and 618.0 kJ/mol for 1C.

The product distribution in amination was analyzed by NMR for 4wt% Au/TiO₂ (Table 5). Besides the anticipated products the mixture contained also 9% unreacted cyclohexanone. The molar ratio between unreacted benzylamine to cyclohexanone was 0.44 showing that amine not only reacts with a ketone, but also undergoes

self- condensation forming *E*-(*N*)-benzyl-1-phenylmethanimine (Table 5). Kinetics of amine formation over different catalysts is shown in Fig. 7.

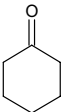
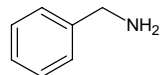
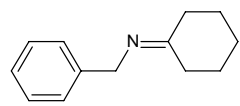
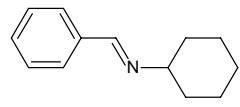
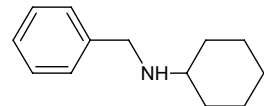
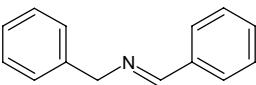
The results illustrate that the lowest produced total concentration is obtained for 4wt% Au/La₂O₃/TiO₂, which exhibited also a high amount of strong acid sites (Table 2). The highest initial rate for amine formation was obtained by 4wt% Au/TiO₂ followed by 4wt% Au/CeO₂/TiO₂ (Table 7). The initial formation rates for three other catalysts were very small resulting also in low conversion after 4 h (Fig. 7). The three most active catalysts, 4wt% Au/TiO₂, 4wt% Au/CeO₂/TiO₂ and 4wt% Au/La₂O₃/TiO₂ were retaining their activity also after 1 h reaction time resulting in 72%, 79% and 27% yield of *N*-benzylcyclohexanamine after 4 h. The concentration of amine increased in the liquid phase for other catalysts as follows: 4wt% Au/CeO₂ < 4wt% Au/La₂O₃ < 4wt% Au/TiO₂ < 4wt% Au/CeO₂/TiO₂.

It is important to note here that rather high yields of amine were obtained with the supported gold catalysts containing small gold particle, below 3 nm (Tables 1 and 7). As a comparison with literature, relatively large gold particles, 8.4 nm were active in reductive amination of aldehydes over gold supported on mesoporous silica functionalized by an amine [62]. In that work [62] the reduction was, however, performed at room temperature with a slight excess of the stoichiometric reducing agent, dimethylphenylsilane in 2-propanol as a solvent.

When using molecular hydrogen as a reducing agent, Au/SiO₂-SO₃H catalyst with 4.1 nm gold particles was rather inactive in reductive amination of furfural with aniline under 50 bar hydrogen at room temperature in ethyl acetate, giving mainly imine and only 3% yield of amine in 8 h [63]. In the latter study the gold particle size was rather large, 4.1 nm, which can decrease the hydrogenation rate as activity of gold catalysts is typically very sensitive to the cluster size. Moreover, a low BE of 83.4 eV indicated the presence of Au^{δ-} [63], while in the current work gold was mainly in the metallic state (Table 4).

The catalyst giving the highest yield for the desired amine, i.e. 4wt% Au/CeO₂/TiO₂ contained twofold more basic sites and 1.3 fold more acidic sites in comparison with 4wt% Au/TiO₂ (Tables 2, 3). A lower amine yield was obtained with 4wt% Au/LaO₂/TiO₂ which also exhibited 2.5 fold strong acid sites in comparison with 4wt% Au/CeO₂/TiO₂. When comparing the amount of strong acid sites for these catalysts and the corresponding amine yields, it can be stated that a lower amount of strong acid sites was beneficial for amine production. It can also be noted that a large fraction of metallic gold exists in 4wt% Au/TiO₂ and 4wt% Au/CeO₂/TiO₂ and 4wt% Au/La₂O₃/TiO₂. The latter one exhibited a lower activity compared to the two former ones, despite a larger amount of metallic gold. 4wt% Au/TiO₂ was more active, but less selective than 4wt% Au/CeO₂/TiO₂.

Table 5 NMR results from reductive amination of cyclohexanone with benzylamine over 4wt% Au/TiO₂

Compound	Yield (%)
 Cyclohexanone (1A)	Conversion 91%
 Benzylamine (1B)	(a)
 <i>N</i> -(cyclohexylmethyl)-1-phenylpropan-1-imine (1C)	6
 <i>(E)</i> - <i>N</i> -(cyclohexylmethyl)-1-phenylpropan-1-imine (1D)	11
 <i>N</i> -benzylcyclohexanamine (1E)	72
Unknown (1G)	8
 <i>(E)</i> - <i>N</i> -benzyl-1-phenylmethanimine (1F)	(b)

(a) The amount of unreacted benzylamine to propiophenone was 0.44

(b) Benzylamine amount and its product excluded from cyclohexanone yield calculation

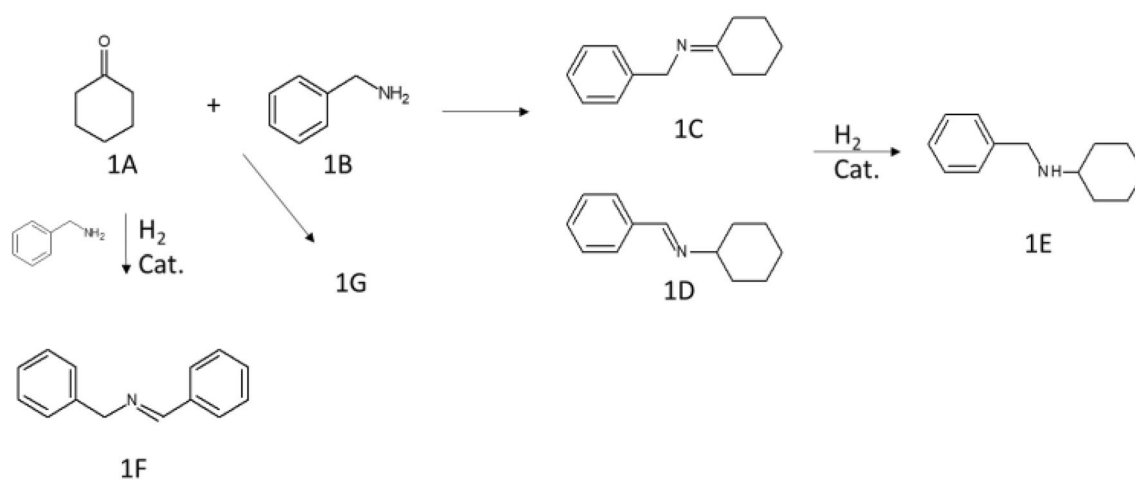
**Fig. 5** The reaction scheme for the reductive amination of cyclohexanone with benzylamine. Notation is in Table 5

Fig. 6 Optimized structures of imines 1D (right) and 1C (left). Bond lengths are given in Ångström

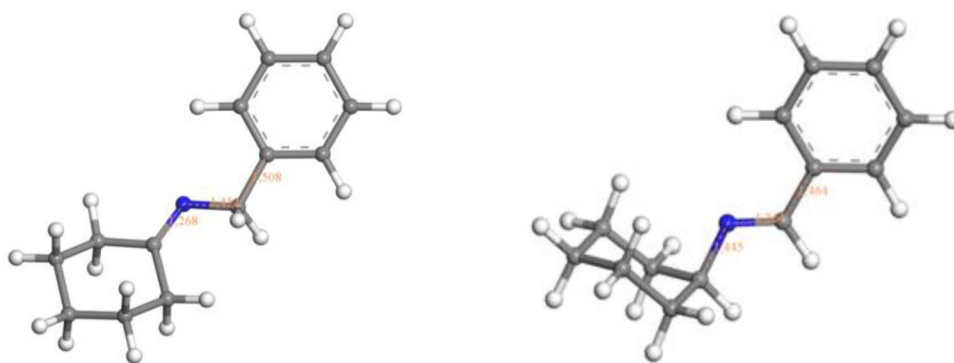


Table 6 Quantum mechanically calculated thermodynamic quantities of imines 1C and 1D

T (K)	Entropy S (cal/mol*K)	Heat capacity Cp	Enthalpy H (kcal/mol)	Free energy G
275.00	106.151	46.679	178.404	149.212
298.15	110.090	50.860	179.533	146.709
300.00	110.406	51.196	179.627	146.505
325.00	114.684	55.753	180.964	143.692
350.00	118.982	60.288	182.415	140.771
375.00	123.294	64.751	183.978	137.743
400.00	127.612	69.102	185.651	134.606
425.00	131.929	73.312	187.432	131.362
450.00	136.235	77.364	189.316	128.010
475.00	140.522	81.248	191.299	124.551
275.00	103.117	45.870	179.042	150.685
298.15	106.991	50.058	180.153	148.253
300.00	107.301	50.396	180.246	148.055
325.00	111.516	54.965	181.563	145.320
350.00	115.756	59.516	182.994	142.479
375.00	120.015	63.998	184.538	139.532
400.00	124.286	68.370	186.193	136.478
425.00	128.559	72.603	187.955	133.318
450.00	132.825	76.679	189.821	130.050
475.00	137.076	80.588	191.788	126.677

In addition to imine and amine, several other products were also identified by NMR (Table 5). No cyclohexanol was observed in the reaction mixture after 4 h for reductive amination of cyclohexanone with benzylamine in toluene on 4wt% Au/TiO₂ opposite to the results where reductive amination was performed in water using a homogeneous reducing agent, such as NaBH₄ and water as a solvent [64]. Absence of cyclohexanol among the products in reductive amination of cyclohexanone with benzylamine in the current work can be partially explained by low ability of metallic gold, produced via reduction with hydrogen at 300 °C, to dissociate hydrogen [65].

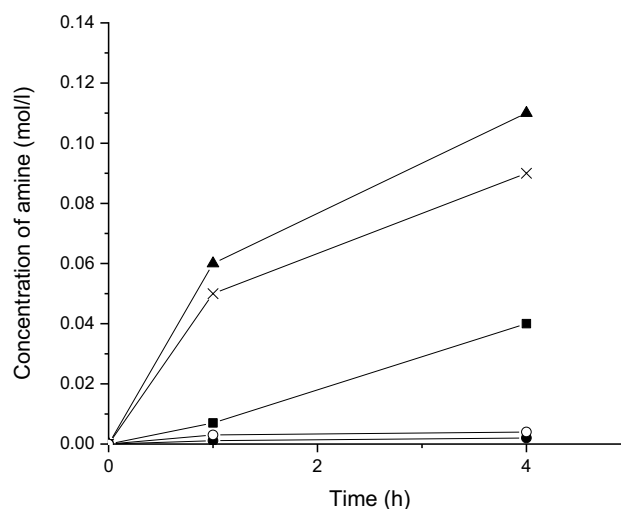


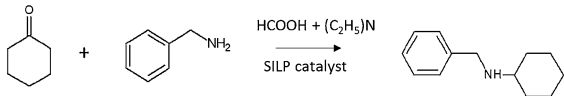
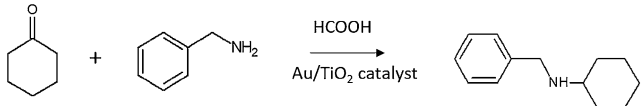
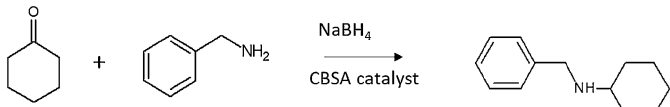
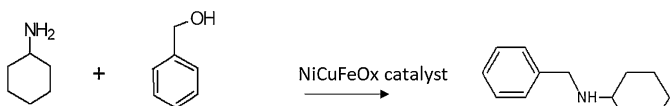
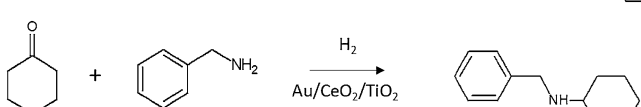
Fig. 7 Concentrations of amine as a function of time in reductive amination of cyclohexanone with benzylamine at 100 °C under 30 bar hydrogen. Notation: (filled triangle) Au/CeO₂/TiO₂, (filled circle) Au/La₂O₃, (open circle) Au/CeO₂, (filled square) Au/La₂O₃/TiO₂ and (x) Au/TiO₂. Catalyst amount 100 mg, the initial concentrations of reactants were 0.13 mol/l

Low activity of 4wt% Au/La₂O₃/TiO₂ is related to its high acidity and basicity. From the mechanistic point of view reductive amination of ketones proceeds differently than amination of alcohols through borrowing hydrogen. In the latter case some acidity is required for dehydrogenation of an alcohol and formation of a corresponding aldehyde. For reductive amination of ketones, it has been stated that the carbonyl bond is activated by homogeneous Lewis acid catalysts, forming an aminol followed by activation of the imine towards nucleophilic attack [64]. Furthermore, it was proposed in ref. [65] for reductive amination of benzaldehyde with aniline using heterogeneous B(OSO₃H)₃/SiO₂ as a catalyst, that Brønsted acidity plays a role in increasing the electrophilic character of the carbonyl compound leading to formation of an intermediate which further dehydrates to imine.

Table 7 The results from reductive amination of cyclohexanone with benzylamine over different catalyst at 100 °C under 30 bar hydrogen

Catalyst	Initial hydrogenation rate (mmol/min/g _{cat})	Conversion after 4 h (%)	Yield of amine after 4 h (%)	Yield of imine after 4 h (%)	Other after 4 h (%)
4wt%Au/TiO ₂	0.4	91	72	17	11
4wt%Au/La ₂ O ₃	Very small	90	2	69	29
4wt%Au/CeO ₂	Very small	89	3	64	33
4wt%Au/La ₂ O ₃ /TiO ₂	0.08	89	27	31	58
4wt%Au/CeO ₂ /TiO ₂	0.5	89	79	10	11

Table 8 Comparison of different methods for production of *N*-benzylcyclohexanamine

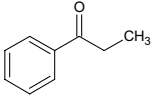
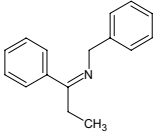
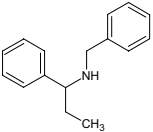
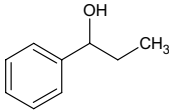
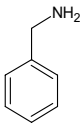
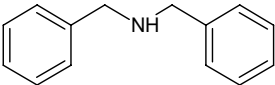
Entry	Reaction	Conditions	Time (min)	Yield (%)	Ref.
1		40 °C, acetonitrile	300	30	[3]
2		70 °C, <i>tert</i> -butanol	300	97	[6]
3		25 °C, no solvent	10	90	[10]
4		138 °C, xylene	1440	89	[8]
5		100 °C, 30 bar, toluene	240	79	This work

Selectivity in amination has also been correlated with electronegativity of the support metal ions in [28, 30]. The results of [28] in amination of myrtenol showed that gold supported on La₂O₃ and CeO₂ exhibited low conversion and selectivity to secondary amines, whereas in *N*-alkylation of aniline with benzyl alcohol the selectivity to secondary amine was slightly higher with Ti⁴⁺ ion in comparison to Ce⁴⁺ ion [30]. The electronegativity of Ti⁴⁺, Ce⁴⁺ and La³⁺ is decreasing as follows: 14, 10 and 8.23, respectively [28, 30]. In reductive amination of cyclohexanone with benzylamine the highest amine yield was obtained over 4wt%Au/TiO₂ with the highest support ion electronegativity in comparison to CeO₂ and La₂O₃, which gave low amine yields. The best catalysts in the current work are Au/TiO₂ and Au/CeO₂/TiO₂ which could also be related to their high electronegativity.

As a comparison the yields of *N*-benzylcyclohexanamine produced via reductive amination (Table 8, entries 1–3)

and *N*-alkylation of cyclohexylamine with benzylalcohol (Table 8, entry 4) with the current results (Table 8, entry 5) agree very well with the work of Liang et al. [6]. In the latter work it was reported that a commercial 1 wt% Au/TiO₂ with 2–3 nm Au particles was very active and selective for production of *N*-benzylcyclohexanamine using 1:4 molar ratio of cyclohexanone to benzylamine with formic acid as a reductant at 60 °C in *tert*-butanol as a solvent giving after 5 h 97% yield of amine [6]. The TOF for formation of *N*-benzylcyclohexanimine, defined as moles of formed amine divided by moles of the surface gold over 1 wt% Au/TiO₂ [6] was 1.1 s⁻¹, while in the current work it was 52 s⁻¹. The main difference between these studies is the use of formic acid as a reducing agent [3, 6], whereas hydrogen was applied in the current study. The gold particle size was about the same in the current work and in [6]. In addition to formic acid [3, 6], also NaBH₄ [10] has been used as a reducing agent for production of *N*-cyclohexylbenzylamine

Table 9 NMR results from the reaction mixture obtained from reductive amination of propiophenone reaction with benzylamine over 4 wt% Au/CeO₂/TiO₂ in cyclohexane as a solvent, 100 °C, 30 bar hydrogen after 5 h

Structure	Yield (%)
 propiophenone (2A)	Conversion 20%
 α-ethyl-N-(phenylmethyl)-benzene-methanimine (2C/2D)	3.2 + 1.1
 α-ethyl-N-(phenylmethyl)-benzene-methanamine (2E)	11.2
 Phenyl-1-propanol (2F)	2
Unidentified  benzylamine (2B)	3.3 (a)
 N-benzylmethanamine (2I)	(a, c)

(a) Benzylamine amount and its product are excluded from cyclohexanone yield calculation

(b) The amount of unreacted benzylamine to propiophenone was 0.48

(c) Very low amount

as illustrated in Table 8. Furthermore, N-alkylation of cyclohexylamine with benzylalcohol is rather slow reaction, although giving a high yield of the desired product (Table 8, entry 4). Thus it can be concluded that Au/CeO₂/TiO₂ using hydrogen as a reducing agent can be considered as a viable alternative to chemical reducing agents.

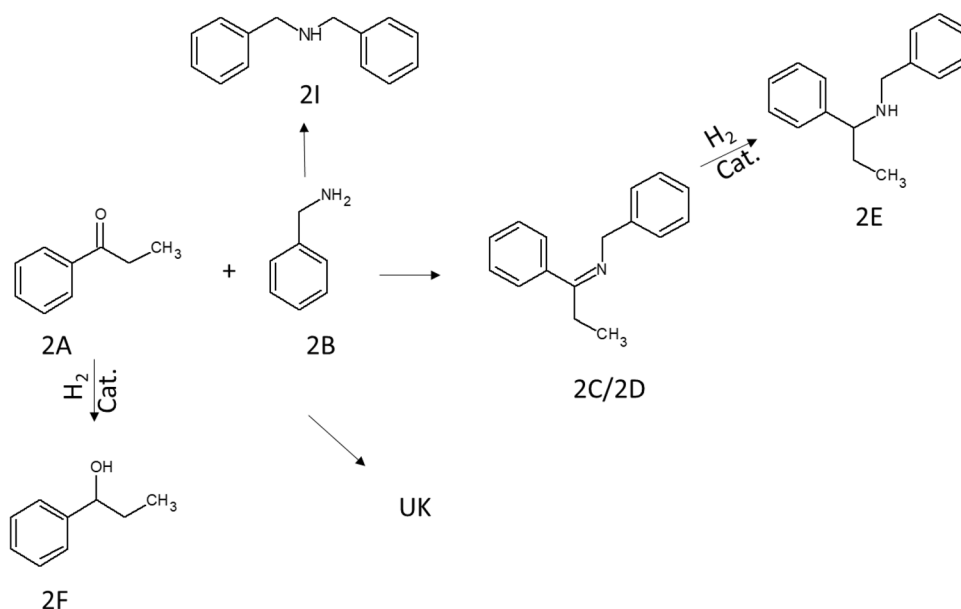
3.2.2 Reductive Amination of Propiophenone

In reductive amination of propiophenone with benzylamine the initial reaction mixture was analyzed by GC-MS showing that a small fraction of propiophenone

has already reacted to the corresponding imine, α-ethyl-N-(phenylmethyl)benzenemethanimine (2C/2D) at room temperature. Together with this imine a small amount of E-(N)-benzyl-1-phenylmethanimine was also present in the initial mixture and the molar ratio between the unreacted benzylamine to propiophenone was 0.48.

Reductive amination of propiophenone over 4wt% Au/CeO₂/TiO₂ resulted in 20% conversion after 4 h (Table 9, Fig. 8). The ratio of unreacted benzylamine to propiophenone over this catalyst was 0.5 showing the benzylamine reacts not only with propiophenone. The yield of the

Fig. 8 The reaction scheme in the reductive amination of propiophenone with benzylamine over 4wt% Au/CeO₂/TiO₂. The notation is the same as in NMR results (Table 9)



desired amine was 11.2% corresponding to TOF of 6.3 s⁻¹ for formation of amine.

The formed imines (2C/2D) were to a substantial extent hydrogenated to the corresponding amine (2E) over 4wt% Au/CeO₂/TiO₂. The final amine selectivity at 20% conversion was 56%, defined as the yield of amine divided by converted propiophenone determined based on NMR analysis. It is known that especially Brønsted acidity promoted the reaction between aniline and furfural under 50 bar hydrogen at room temperature in ethyl acetate [50], when the imine was formed in the first step followed by hydrogenation to corresponding amine.

Hydrogenation of the carbonyl bond in ketone was very minor, 2% yield, over 4wt% Au/CeO₂/TiO₂ catalyst in comparison to formation of imine with subsequent hydrogenation to amine, which was analogous to the case of cyclohexanone reductive amination. In addition to the desired imines, amines and phenyl-1-propanol, minor amounts of unidentified side products were formed (Table 9).

4 Conclusions

Several gold catalysts supported on TiO₂, La₂O₃, CeO₂, and mixed oxides, La₂O₃/TiO₂, CeO₂/TiO₂ were prepared by deposition–precipitation method and investigated in reductive amination of cyclohexanone and propiophenone using molecular hydrogen as a reducing agent. Typically Au was present as small particles, below 3 nm in all other catalysts except Au/CeO₂ which had a slightly larger cluster size. According to XPS gold mainly the metallic state after pre-reduction with hydrogen at 300 °C. The lowest fraction of metallic Au was present in Au/La₂O₃ catalysts.

The catalytic results revealed that the most promising catalysts in reductive amination of cyclohexanone with benzylamine at 100 °C under 30 bar hydrogen using toluene as a solvent namely 4 wt% Au/CeO₂/TiO₂ exhibited mainly weak and medium strong acid sites. On the other hand, 4 wt% Au/La₂O₃/TiO₂ was very unselective catalyst giving only 27% yield of *N*-benzylcyclohexanamine at 89% conversion. This catalyst contained mainly strong acid sites. The best catalyst in amination of cyclohexanone, 4 wt% Au/CeO₂/TiO₂, was also tested in reductive amination of propiophenone giving 56% selectivity to corresponding amine at 20% conversion in 5 h.

Acknowledgements Open access funding provided by Abo Akademi University (ABO). The research is funded from Tomsk Polytechnic University Competitiveness Enhancement Program project VIU-RSCBMT-65/2019.

Compliance with Ethical Standards

Conflict of interest The authors declare no conflict of interest.

Open Access This article is distributed under the terms of the Creative Commons Attribution 4.0 International License (<http://creativecommons.org/licenses/by/4.0/>), which permits unrestricted use, distribution, and reproduction in any medium, provided you give appropriate credit to the original author(s) and the source, provide a link to the Creative Commons license, and indicate if changes were made.

References

1. Heutling A, Pohlki F, Doye S (2004) Chem Eur J 10:3059–3071
2. Gandon V, Bertus P, Szymoniak J (2001) Eur J Org Chem 2001:3677–3681

3. Tamboli AH, Chaugule AA, Chun WJ, Kim H (2015) *Chin J Catal* 36:1365–1371
4. Ou W, Han F, Hu XN, Chen HPQ, Huang PQ (2018) *Angew Chem Int Ed* 57:11354–11358
5. Chusov D, List B (2014) *Angew Chem Int Ed* 53:5199–5201
6. Liang S, Mosen P, Hammond GB, Xu B (2016) *Org Chem Front* 3:505–509
7. Werkmeister S, Junge K, Beller M (2012) *Green Chem* 14:2371–2374
8. Cui X, Dai X, Deng Y, Shi F (2013) *Chem Eur J* 19:3665–3675
9. Hara M, Yoshida T, Takagaki A, Takata TK, Kondo JN, Hayashi S, Domen K (2004) *Angew Chem Int Ed* 43:2955–2958
10. Shokhoralı A, Zali A, Keshavarz MH (2011) *Green Chem Lett Rev* 4(3):195–203
11. Pan HJ, Ng TW, Zhao Y (2016) *Org Biomol Chem* 14(24):5490–5493
12. Zanella R, Louis C, Giorgio S, Touroude R (2004) *J Catal* 223:328–339
13. Inorganic Crystal Structure Database (ICSD), version 2.1.0, <http://www.fiz-karlsruhe.de/icسد.html>, October 2018, Fiz Karlsruhe
14. Delley B (1990) *J Chem Phys* 92:508–517
15. Delley B (2000) *J Chem Phys* 113:7756–7764
16. Becke AD (1993) *J Chem Phys* 98:5648–5652
17. Lee C, Yang W, Parr RG (1998) *Phys Rev B* 37:785–789
18. Vosko SH, Wilk L, Nusair M (1980) *Can J Phys* 58:1200–1211
19. Stephens PJ, Devlin FJ, Chabalowski CF, Frisch MJ (1994) *J Phys Chem* 98:11623–11627
20. McNellis ER, Meyer J, Reuter K (2009) *Phys Rev B* 80:205–414
21. Markowska-Szczupak A, Janda K, Wang K, Morawski AW, Kowalska E (2015) *Cent Eur J Public Health* 23(3):198–202
22. Kotolevich Y, Kolobova E, Khramov E, Farías MH, Zubavichus Y, Tiznado H, Martínez-González S, Cortés Corberán V, Motamorales JD, Pestryakov A, Bogdanchikova N (2017) *J Mol Catal A* 427:1–10
23. Seong G, Dejhosseini M, Adshiri T (2018) *Appl Catal A* 550:284–296
24. E. Scharfenberger Mineralogisch-Petrogr. Institut, Universität Heidelberg, Germany, ICDD Grant-in-Aid, 1985
25. Olafsen A, Larsson A-K, Fjellvåg H, Hauback BC (2001) *J Solid State Chem* 158:14–24
26. McMurdie H, Morris M, Evans E, Paretzkin B, Wong-Ng W, Hubbard C (1986) *Powder Diffr* 1:90
27. dal Negro A, Rossi G, Tazzoli V (1975) *Am Miner* 60:280–284
28. Demidova YuS, Simakova IL, Estrada M, Beloshapkin S, Suslov EV, Korchagina DV, Volcho KP, Salakhutdinov NF, Simakov AV, Murzin DYu (2013) *Appl Catal A* 464–465:348–358
29. Shimizu K, Nishimura M, Satsuma A (2009) *ChemCatChem* 1:497–503
30. Ishida T, Takamura R, Takei T, Akita T, Haruta M (2012) *Appl Catal A* 413–414:261–266
31. Nayak VS, Chodhary VR (1983) *J Catal* 81(1):26–45
32. Olson DH, Kokotailo GT, Lawton SL, Meier WM (1981) *J Phys Chem* 85(15):2238–2243
33. Zhu M, Zeng Y, Zhang Sh, Deng J, Zhong Q (2017) *J Environ Sci* 54:277–287
34. Pakrieva E, Kolobova E, Mamontov G, Bogdanchikova N, Farias MH, Pascual L, Cortés Corberán V, Martínez Gonzalez S, Carabineiro SAC, Pestryakov A (2019) *ChemCatChem* 11(6):1615–1624
35. Kubicka D, Kumar N, Mäki-Arvela P, Tiitta M, Niemi V, Karhu H, Salmi T, Murzin DY (2004) *J Catal* 227:313–327
36. Kubicka D, Kumar N, Venäläinen T, Karhu H, Kubickova I, Österholm H, Murzin DYu (2006) *J Phys Chem B* 110:4937–4946
37. Villegas JL, Kubicka D, Karhu H, Österholm H, Kumar N, Salmi T, Murzin DYu (2007) *J Mol Catal A* 264:192–201
38. Zanella R, Giorgio S, Henry CR, Louis C (2002) *J Phys Chem B* 106:7634–7642
39. Hinojosa-Reyes M, Camposeco-Solis R, Zanella R, Rodríguez-González V, Ruiz F (2018) *Catal Lett* 148:383–396
40. Zanella R, Delannoy L, Louis C (2005) *Appl Catal A* 29:62–72
41. Zanella R, Louis C (2005) *Catal Today* 107–108:768–777
42. Chichova D, Mäki-Arvela P, Heikkilä T, Kumar N, Väyrynen J, Salmi T, Murzin DYu (2009) *Top Catal* 52:359–379
43. Thanh DN, Kikhtyanin O, Ramos R, Kothari M, Ulbrich P, Munshi TD, Kubicka D (2016) *Catal Today* 277:97–107
44. Di Cosimo JL, Diez VK, Xu M, Iglesia E, Apesteguia CR (1988) *J. Catal.* 178:499–510
45. Di Serio M, Ledda M, Cozzolino M, Minutillo G, Tesser R, Santacesaria E (2006) *Ind Eng Chem Res* 45:3009–3014
46. Veloso CO, Pérez CN, de Souza BM, Lima EC, Dias AG, Monteiro JLF, Henriques CA (2008) *Microporous Mesoporous Mater* 107:23–30
47. Martínez-Ramírez Z, González-Calderon JA, Almendarez-Camarillo A, Fierro-Gonzalez JC (2012) *Surf Sci* 606:1167–1172
48. Pestryakov AN, Lunin VV, Kharlanov AN, Bogdanchikova NE, Tuzovskaya IV (2003) *Eur Phys J D* 24:307–309
49. Feldheim DL, Foss CA (2002) *Metal nanoparticles: synthesis characterization and applications*. Basel Marcel Dekker Inc, New York, p 338
50. Costa VV, Estrada M, Demidova Y, Prosvirin I, Kriventsov V, Cotta RF, Gusevskaya EV (2012) *J Catal* 292:148–156
51. Feng R, Li M, Liu M (2012) *Coll Surf A* 406:6–12
52. Guzmán C, del Ángel G, Gómez R, Galindo-Hernández F, Ángeles-Chavez C (2011) *Catal Today* 166:146–151
53. Galindo-Hernández F, Wang JA, Gómez R, Bokhimi X, Lartundo L, Mantilla A (2012) *J Photochem Photobiol A* 243:23–32
54. Penkova A, Chakarova K, Laguna OH, Hadjiivanov K, Saria FR, Centeno MA, Odriozola JA (2009) *Catal Commun* 10:1196–1202
55. Peters S, Peredkov S, Neeb M, Eberhardt W, Al-Hada M (2013) *Surf Sci* 608:129–134
56. Llorca J, Domínguez M, Ledesma C, Chimentão RJ, Medina F, Sueiras J, Rossell O (2008) *J Catal* 258:187–198
57. Veith GM, Lupini AR, Pennycook SJ, Ownby GW, Dudley NJ (2005) *J Catal* 23:151–158
58. Wagner ME, Davis G, Müllenberg G (1979) *Handbook of X-ray Photoelectron Spectroscopy*. Perkin-Elmer Corp. Physical Electronics Division, Eden Prairie, p 190
59. Figueiredo NM, Carvalho NJM, Cavaleiro A (2011) *Appl Surf Sci* 257:5793–6926
60. Pawelec B, Castano P, Zepeda TA (2008) *Appl Surf Sci* 254:4092–4102
61. Tuzovskaya I, Bogdanchikova N, Simakov A, Gurin V, Pestryakov A, Avalos M, Farías MH (2007) *Chem Phys* 338:23–32
62. Carrilo AI, Llanes P, Pericas MA (2018) *React. Chem Eng* 3:714–721
63. Martínez JJ, Nope E, Rojas H, Brijaldo MH, Passos F, Romanelli GJ (2014) *J Mol Catal A* 392:235–240
64. Jones AB, Studies towards combined chemo-biocatalytic reactions in water. University College London, doctoral thesis, 2011, 356
65. Alinezhad H, Tajbakhsh M, Hamidi N (2010) *Turk J Chem* 34:307–312

Publisher's Note Springer Nature remains neutral with regard to jurisdictional claims in published maps and institutional affiliations.

Affiliations

E. Kolobova¹ · P. Mäki-Arvela² · A. Pestryakov¹ · E. Pakrieva¹ · L. Pascual³ · A. Smeds² · J. Rahkila⁴ · T. Sandberg⁵ · J. Peltonen⁶ · D. Yu. Murzin²

¹ Research School of Chemistry & Applied Biomedical Sciences, Tomsk Polytechnic University, Lenin Avenue 30, Tomsk, Russia 634050

² Johan Gadolin Process Chemistry Centre, Abo Akademi University, 20500 Turku, Finland

³ Institute of Catalysis and Petroleum Chemistry (ICP), CSIC, Marie Curie 2, 28049 Madrid, Spain

⁴ Instrument Centre, Åbo Akademi University, 20500 Turku, Finland

⁵ Laboratory of Physical Chemistry, Abo Akademi University, 20500 Turku, Finland

⁶ Laboratory of Industrial Physics, University of Turku, 20014 Turku, Finland